Electronic Supplementary Material (ESI) for Journal of Analytical Atomic Spectrometry.
This journal is © The Royal Society of Chemistry 2020

Appendix

Illustrations that Explain Issues Encountered Quantifying SIMS Analysis due to Matrix Effects in DLC

A. Spatial Variations in ion yields and density

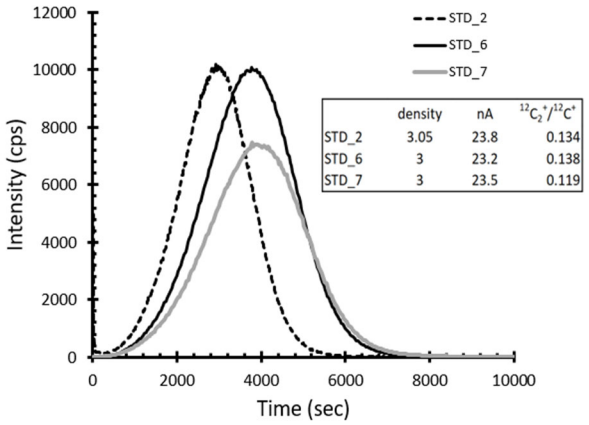

FIG. A1. *Three profiles from the standard analyzed under the same conditions.*

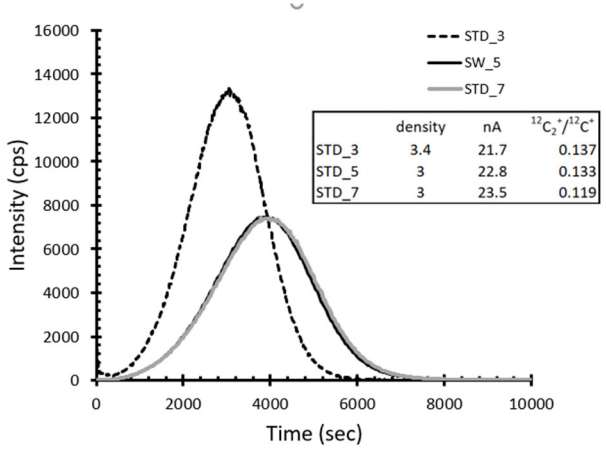

FIG.A2. *Three profiles from the standard analyzed under the same conditions, but one has a significantly different density.*

FIG. 2 in the text showed how the ion yields from analyses of the standards varied with the amount of DLC removed per cm^3 per nA. However, when sitting in the SIMS facility, what is observed is much more striking. FIG. A1 gives depth profiles (^{25}Mg, raw data) from three analyses taken under the same conditions on the same implant standard (average beam current within 0.5 nA). Moreover, the SRIM fit gives effectively the same density for all three. STD_2 has a faster sputtering rate because it reactively etches; STD_7 has a slow sputtering rate and intensities show the effect of minor silicon; STD_6 plotted closest to the vertical line in FIG. 2, and has some properties of both types of sputtering. FIG. A2 also gives depth profiles (^{25}Mg, raw data) from three analyses taken under same conditions on the same implant standard. The average beam current varies almost 1.5 nA, but the analysis with lowest beam current (STD_3) shows the highest intensity. Note that the density of STD_3 also has an anomalously high density.

The differences in profile shapes, positions and intensity are striking. Accordingly, testing the accuracy of the SIMS analysis in real time is problematic. Since the beam current is nearly constant, many analysts would assume that the sputtering rate and ion yields should be constant. The analysts would then likely infer that either the implant is non-uniform or that there is something wrong with the SIMS.

To once more emphasize the unusual features of depth profiles in DLC, Fig. A3 gives a different perspective: two model depth profiles with the same nominal SRIM matrix with

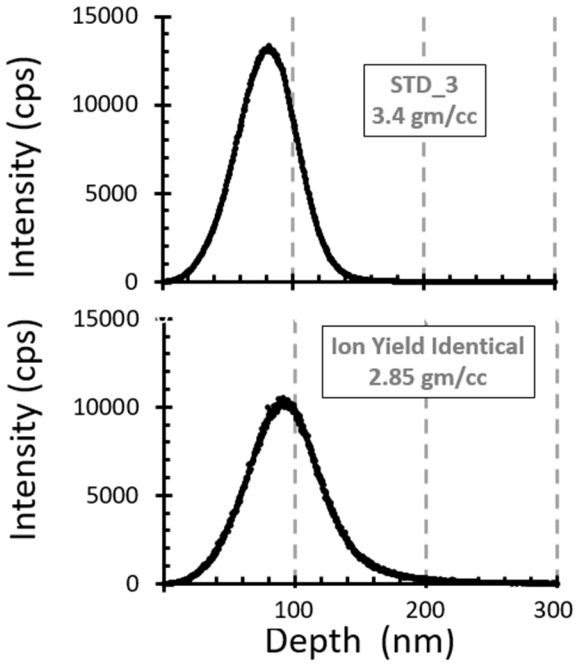

FIG. A.3*. Models using the same matrix having different densities. Vertical lines are for reference.*

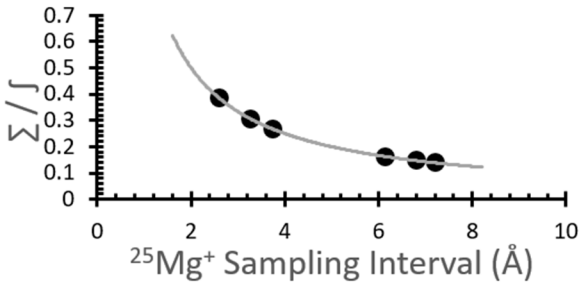

FIG. A.4*. (sum/integral) ratios using our six standard analyses. Two different sets of counting times (e.g., duty cycles) were used. The line just emphasizes differences.*

different densities. Specifically, both analyses are in matrices that are very diamond-like (see FIG. 4 in text and SRIM-fit discussion in *Section D* of this online Appendix). One model is based on STD_3, the other is based on STD_4, but the intensity has been normalized so that the area under the curve is the same as for STD_3. Dashed vertical lines have been added to the plots simply for reference. If you kept the SIMS conditions as constant as possible, sputtering rates (depth/time) would still be different since the matrices have different densities. Moreover, inspection of the two curves shows that not only are the peaks in different locations, but the highest count for each is still different because STD_4 is slightly broader than STD_3 and the areas under the curve ($^{25}Mg^+$ generated per ^{25}Mg atom in the implant) is a constant. This difference would definitely cause issues if you were sitting at the SIMS trying to figure out if you were getting the same number of counts per profile. That is, if you summed the counts you collected per unit time, the two profiles would still give different numbers, even though the true integrals under the curve are identical. For example, if you only took two counts per depth profile (at the positions of the vertical lines), then the counts at 100 nm are about 14500 with "no" counts at 200 nm in STD_3, but about 10500 at 100 nm and 300 at 200 nm in the STD_4-based model. Of course, taking two measurements per depth profile is extreme, and the SIMS duty cycles give a much greater the sampling rate. The more duty cycles (i.e., samples of the $^{25}Mg^+$ curve), the closer the proportionality of the sum of the counts (∑) to the area under the curve (depth integral or ∫). Still, except at the limit where the sampling rate goes to 0, there will be a finite difference between the two sums if you use the same duty cycle, and this difference can be large. Again, using analyses of our DLC implant standard as an example, this effect is illustrated in FIG. A.4. The power-law "trendline" is given to emphasize that the variation in the ratio fits the ratios for this data set well. Note, however, that it is not correct, as the equation goes to infinity at x=0, while, in fact, $(\lim_{dx\to 0} \sum_{x=0}^{\infty} (^{25}Mg^+(x)))/(\int {}^{25}Mg^+(x)\, d\, x) = 1$.

B. Textural Changes with Depth and their Lack of Effect on Electrical Conductivity

As discussed in the part above and in the text, the electrical conductivity varies laterally across individual DoS (diamond-like carbon on silicon) wafers, as will be further detailed in section C. Although it is plausible that conductivity may also vary with depth, that effect has not been observed in our work when the $^{12}C_2^+/^{12}C^+$ ratio (a proxy for the electrical conductivity) was monitored with depth, nor in the work of Sullivan et al. [1]. Electrical conductivity appears to be constant true even though the texture of the films is clearly not uniform with depth, as shown in FIG. B.1.

FIG. B.1 shows two Raman Spectra: one from the surface adjacent to an analysis crater on a Genesis flown sample (brown); the second at the bottom of that same analysis crater (black). Therefore, brown spectrum gives the "full" depth (emphasizing the upper portion of the DLC film), while the black spectrum gives the texture deeper than 410 nm of the matrix only. Note that the intensity of the G and D peaks (which reflect bonding and texture, see Ref. [2]) are different. Another analysis which also clearly had spatial differences in composition within the column of matrix was STD_3, an analysis into matrix that contained crystals. For STD_3, the $^{12}C^+$ and $^{12}C_2^+$ show fluctuations with depth, mainly near the zones that were surfaces during annealing (FIG. B.2). Yet, the electrical conductivity, as represented by the $^{12}C_2^+/^{12}C^+$ ratio, is constant.

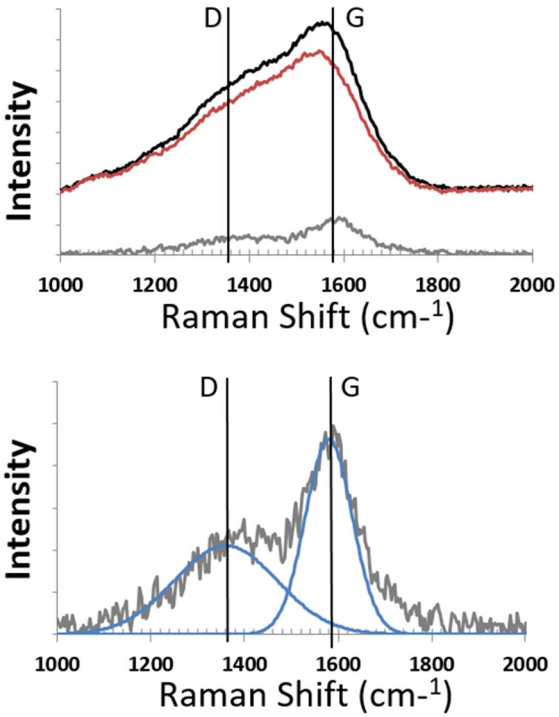

FIG. B.1*. (top) Raman spectrum from the surface adjacent an analysis crater (brown), vs a second spectrum from the bottom of the crater (black). Note the differences in the D and G peaks (gray; bottom).*

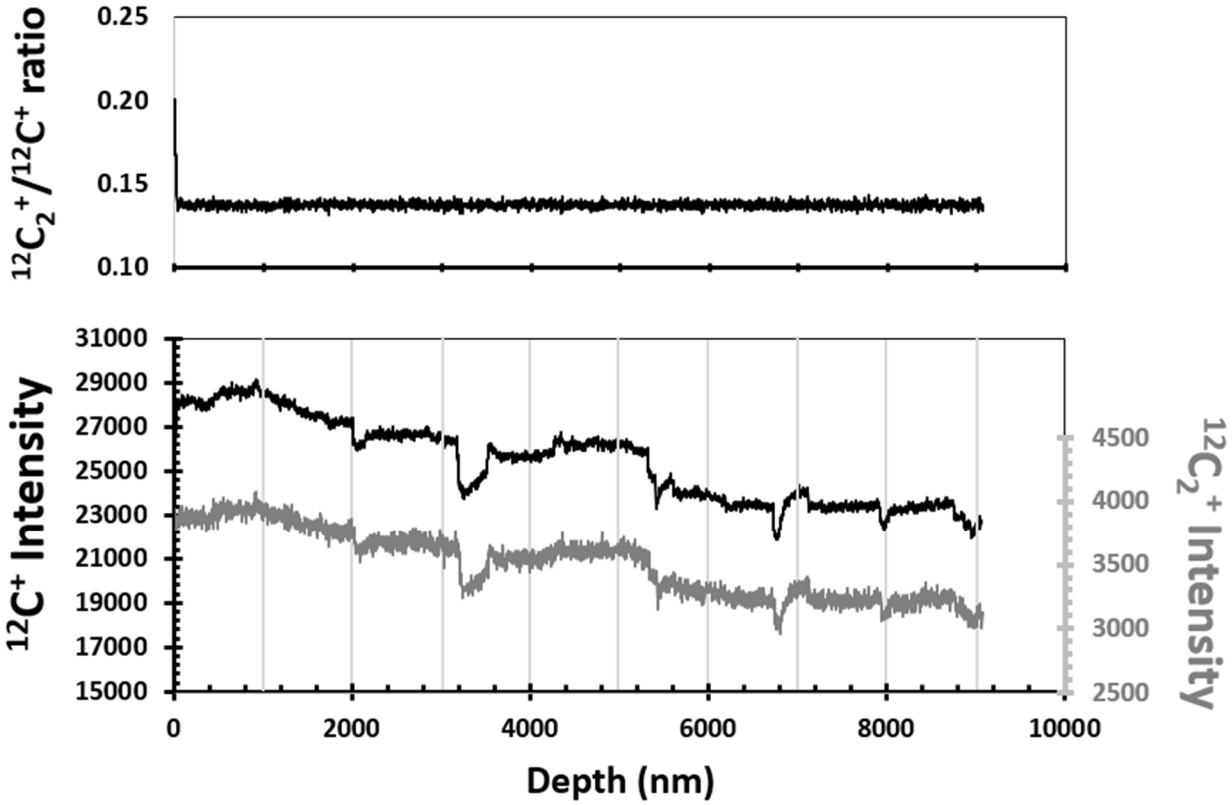

***FIG. B.2**. Depth profiles for $^{12}C_2^+$ (grey) and $^{12}C^+$ (black), as well as their ratio with depth, as measured in STD_3. Fluctuations in the intensity roughly correspond with the buried DLC surfaces that were during the intermittent anneals (i.e., every 100-120nm); however, the ratio of the intensities of the ions is a constant. This uniformity in the $^{12}C_2^+/^{12}C^+$ ratio crystals exists even though diamond crystals were present in the profiles. So, although the texture of the DLC may change enough to affect the intensity, the conductivity does not change.*

C. A reason for spatial variations in Electrical Conductivity

The work by Sullivan et al. wasn't focused on conductivity vs. location, only electrical conductivity as a function of annealing temperature, residual stress, and time of annealing. But, for any coated wafer, any internal stress in the coating will be a function of position. FIG. C.1 and FIG. C.2 illustrate this fact.

FIG. C.1. shows two DoS wafers with DLC films that show stress birefringence. In both cases, the rings are not parallel to the edges of the DLC nor precisely centered inside the wafer. Notice also that the rings in (a) are slightly elliptical and the rings in (b) are squares with rounded corners. Rings that were caused by different thicknesses (i.e., less deposition at distances further from the source) would be round. The birefringence was not observed in all of the flight DoS wafers. It is likely that the visibility of the birefringence depends both upon

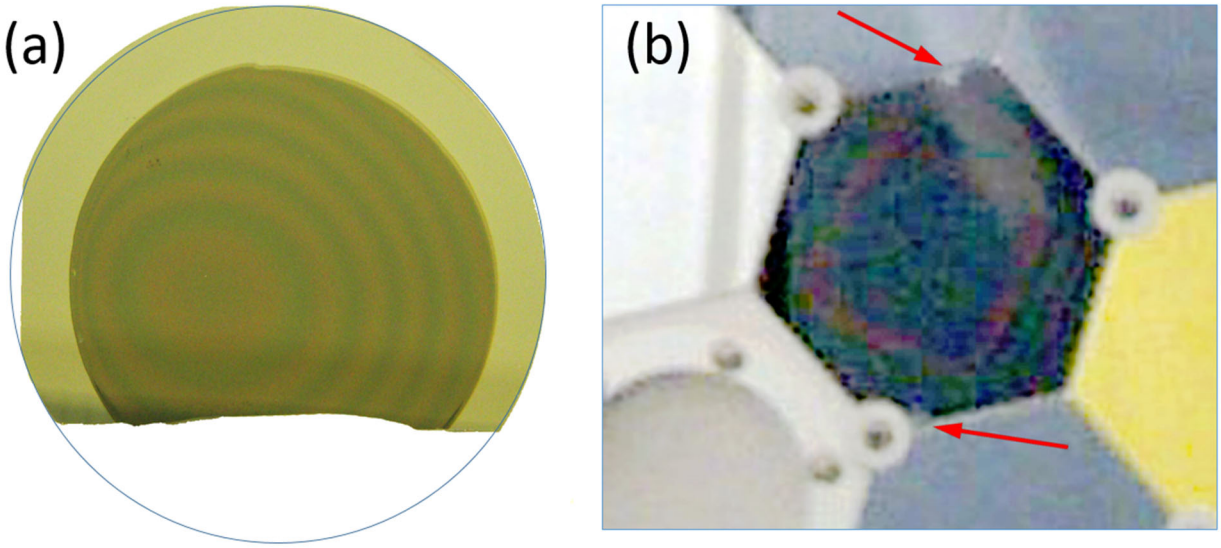

FIG. C.1*. Two DoS wafers showing stress birefringence. (a) Photo of a test wafer. Circle is for reference; photo has been stretched slightly to mitigate camera parallax. Note that center ring is oval and offset from the center of the wafer. (b) Color-enhanced photo of a DoS pre-flight mounted in the L-array. In this hexagonal wafer, the birefringent rings are not round. Red arrows point to the DLC silicon-free clip marks that were exposed during flight. (b) was cropped and enhanced from a photo of the L-array taken during assembly of the Genesis arrays in the Astromaterials Research and Exploration Science group at NASA JSC*

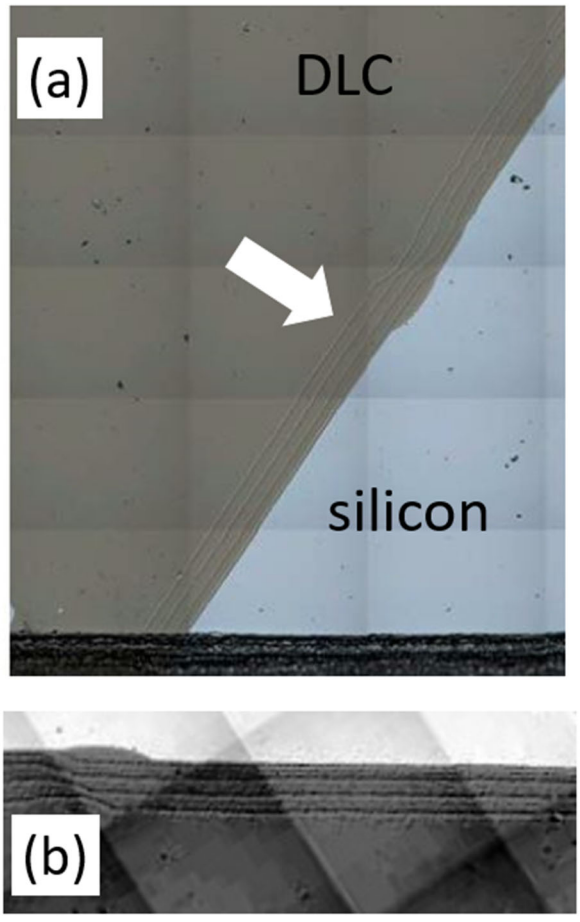

distributed and (2) the final electrical conductivity of a column of DLC is determined primarily by (variable) optical characteristics of the DLC film and, perhaps, the wavelengths and angle of the room lighting. In FIG C.1, the thickness of the two films vary by a factor of 3, again suggesting that birefringence due to film thickness is (at most) a second-order effect.

The separate depositional layers within the DLC are visible at the edges of wafers as "steps" (macro-photographs in FIG. C.2). Because of the compressive stresses within the film, each layer of DLC has slipped slightly relative to the other layers – at least at the edges, where the compressive stress of the DLC

FIG. C.2*. Individual layers of the DLC, which are visible at the edges of wafers. The arrow in (a) points to the area that is enlarged in (b). These photo-mosaics are modified from images taken by Genesis Curation in the Astromaterials Research and Exploration Science group at NASA JSC.*

is acting on a free surface. This slippage was probably during annealing, when the heating allowed some restructuring of the film and likely some minor shrinkage in response to the stresses. Because (1) the internal stress is non-uniformly the magnitude of the stresses, it is not surprising that the electrical conductivity of the DLC varies spatially across the wafer.

D. Matrix Effects due to Electrical Conductivity Variations

Although the electrical conductivity of DLC is effectively constant with depth, it does vary spatially across the film. This assessment was experimentally derived in 1998 by Sullivan et al. (ref. [1]) for DLC fabricated using techniques similar to those used to make DLC for this study. A good mental visualization of electrical conductivity in DLC would be to imagine a columnar growth structure for the film, with each column having a different texture and/or a different proportion of sp^2 and sp^3 carbon bonds. Details related to the electrical conductivity that are specific to the samples and/or analytical conditions studied herein are discussed in both Section C above and in the main text, Section 4.1 *Relevance of the C2+/C+ parametrization*.

The spatial variation of electrical conductivity in DLC ***does*** effect SIMS analyses. In depth profiling mode, the ***shape*** of each depth profile is unaffected because the electrical conductivity is uniform with depth; however, the ***intensity*** of each depth profile changes with the electrical conductivity of the matrix material being sampled. Therefore, the effect of spatial variability of electrical conductivity on SIMS analyses of in DLC is to change the intensity of the measured ions with position on the sample. This effect is shown in FIG. D.1(a), the plot of the intensity of one matrix ion versus that of a second matrix ion. Note that all six of these analyses taken within a 1.5 cm x1.5 cm area on the standard. The data in FIG. D.1(a) have been normalized to beam current intensity, so beam current is not a cause of variable intensities.

FIG. D.1(b) gives the ratio of the same two matrix ions ($^{12}C^+$ and $^{12}C_2^+$) versus voltage offset[3] as measured on DLC from a single point on a DLC film in 2020 (matrix-ion spectra are given in FIG. 6(a) in the main text). Using this plot, if the ratio of the matrix ions for an analysis is known, then the voltage offset of the DLC sampled by that analysis can be calculated. Conversely, if the voltage offset of the matrix of that DLC analysis is known, then the change in intensity of the matrix ions caused by that change in electrical conductivity can be calculated from the energy spectra.

FIG. D.1(c) was modified from the white box of FIG. D.1(b). The modifications highlight aspects of the data that were used in the calculation of voltage offsets for individual analyses ("offset[a]" in Table D.I). Arrows indicate the measured $^{12}C_2^+$ / $^{12}C^+$ for individual depth profiles. The markers are only data used to create the trendline (solid line) -- the equation for this trendline was used to calculate the voltage offset for each $^{12}C_2^+$ / $^{12}C^+$ value (arrow), with the exception of STD_4. STD_4 fell within the red gradient in the upper right-hand corner of the figure (see footnotes of Table D.I). The red gradient indicates $^{12}C_2^+$ / $^{12}C^+$ values in this region of

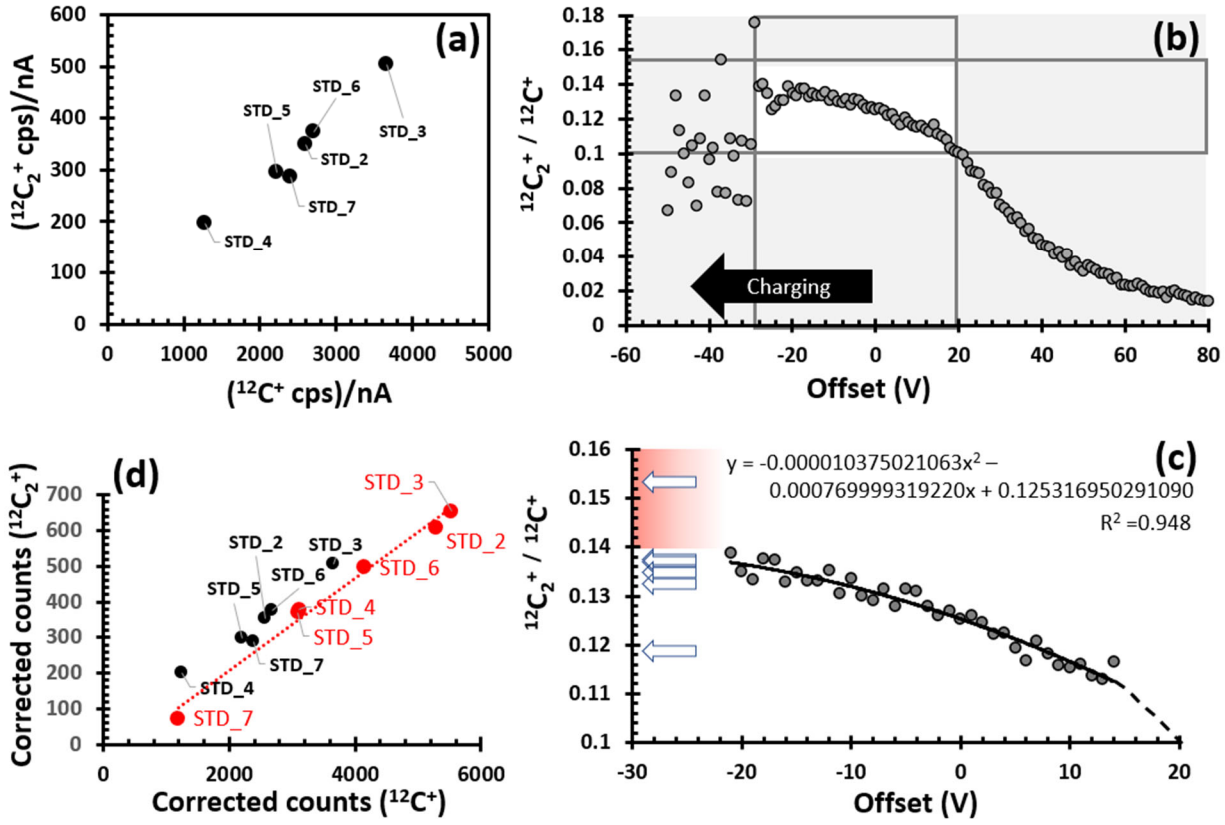

***FIG.D.1**. Determination of the relationship between ion intensity electrical conductivity of the sample. (a) measured matrix ion intensity ($^{12}C_2^+$ and $^{12}C^+$) for the six standards normalized for primary current (after FIG. 3 in text). (b) $^{12}C_2^+$ / $^{12}C^+$ from measure energy spectra versus voltage-offset calculated from energy spectra of FIG. 6 in main text. The voltage offset of the matrix changes with position in the DLC[§]. (c) plot based on the white box in (b): the red gradient marks the onset of secondary-ion signal breakdown due to charging; the dashed line marks the onset of the exponential decrease of the secondary-ion signal; the arrows point to the measured $^{12}C_2^+/^{12}C^+$ of the standards (the highest arrow is STD_4 and the lowest is STD_7). The equation and R^2 are for the solid line (best fit for data used in calculations). Features of (c) are discussed in the Appendix text. (d) intensity of matrix ions for each standard analysis (red - calculated from the energy spectra; black - measured data in FIG. D.1 (a)).*

the plot deviate from the solid trendline. This scattering is due to the onset of signal breakdown due to excessive charge buildup[§§]. Although scattering begins in the white box of FIG. D.1(b), it is more clearly seen in the grey boxes on the left-hand side of the figure. The dashed line (right-hand side of FIG. D.1(c)) is data consistent with the trend in the lower right-hand grey box of FIG. D.1(b), whose rapid drop in intensity can be modeled using an exponential fit.

The calculation for the effect of electrical conductivity on secondary ion intensity is illustrated in FIG. D.2 using $^{12}C^+$. The energy spectrum is that from FIG. 6 in the main text, but the voltage "0 offset" is anchored at STD_3. The choice of STD_3 for the 2009 reference matrix was based on a plausibility argument given in the main text (see description of FIG. 3). The solid lines in FIG. D.2 were best fit polynomial trendlines; using the equations (box below plot), the

intensity at the appropriate offset ("offset[b]" in Table D.I) could be calculated analytically. The results from both $^{12}C^+$ and $^{12}C_2^+$ spectra are included in Table D.I as the (est)[c] intensities.

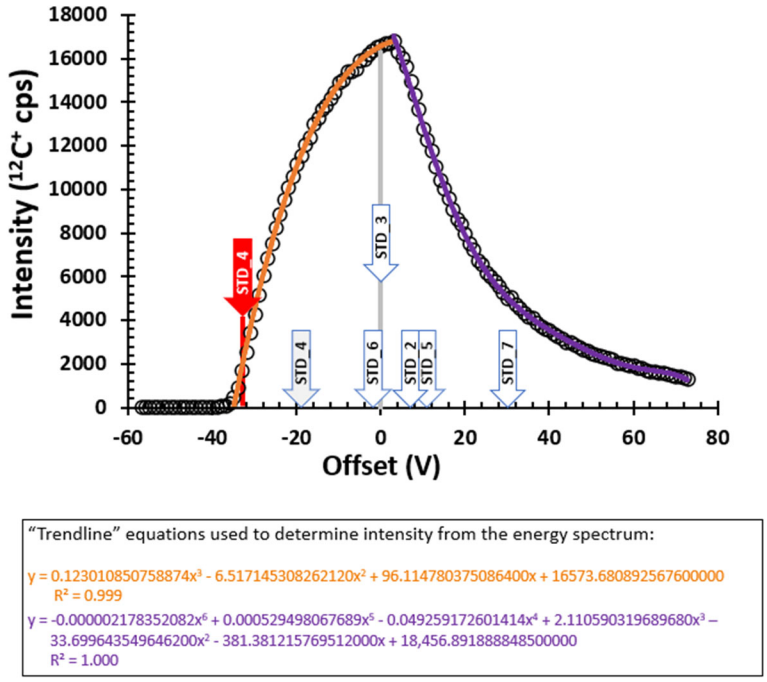

***FIG. D.2**. Measured energy spectrum (markers) with the "0 offset" point set to STD_3 to approximate the 2009 analyses. This change in the point of 0 offset was required because the $^{12}C^+$ and $^{12}C_2^+$ energy spectra were taken in 2020 on a piece of flight spare DLC unrelated to the 2009 analyses.*

FIG. D.2. (as shown) was used in calculation of the intensity of $^{12}C^+$ (est)[c] in Table D.1 for each voltage offset marked by an arrow. The $^{12}C_2^+$ spectrum was treated identically to obtain the (est)[c] data for $^{12}C_2^+$ in Table D.I. Trendline equations (color-coded in box) were used to calculate intensity from the voltage offset ("offset[b]" in Table D.I).

Table D.I. Data table for explanation of calculation for deriving FIG. D.1(d).

	SIMS Data $^{12}C_2^+ / ^{12}C$	offset[a] (V)	offset[b] (V)	$^{12}C^+$ (est)[c]	$^{12}C_2^+$ (est)[c]	Sputter rate (Å/s)	Δ na	Δρ	$^{12}C^+$ (est)[d]	$^{12}C_2^+$ (est)[d]
STD_2	0.1344	-14.78	7.49	16980	1960	0.304	0.99	1.02	5278	609
STD_3	0.1373	-22.26	0.00	16574	1964	0.266	0.90	1.13	5528	655
STD_4[e]	0.1536	-41.97	-19.71	11207	1363	0.211	0.72	0.95	3106	378
STD_5	0.1327	-11.33	10.93	12395	1486	0.238	0.95	1.00	3091	371
STD_6	0.1379	-24.20	-1.94	16362	1963	0.244	0.96	1.00	4140	497
STD_7	0.1187	7.83	30.09	5033	312	0.230	0.98	1.00	1185	73

[a] matrix voltage offset calculated using FIG. D.1(c).
[b] matrix voltage offset calculated assuming that the energy spectra were taken on a matrix like that of STD_3.
[c] estimate of $^{12}C^+$ and $^{12}C_2^+$ intensity using the method given in FIG. D.2.
[d] estimate of $^{12}C^+$ and $^{12}C_2^+$ above corrected for relative primary beam intensity and SRIM model density. These are the results plotted in FIG. D.1(d).
[e] The $^{12}C^+/^{12}C_2^+$ for STD_4 was literally off the chart in FIG. D.1(c) so the value of offset[a] was estimated using a linear extrapolation of the data in FIG. D.1(c) rather than the 2nd order polynomial shown. If, instead of trying to extrapolate an offset, it had been assumed that STD_4 was on the verge of signal failure due to charging (e.g., offset[b] = ~ -33 V), then in FIG. 1(d), STD_4 would have an (est)[d] for ($^{12}C^+$, $^{12}C_2^+$) of (522,2); i.e., approximately the minimum feasible signal.

FIG. D.1(d) and Table D.I gives our results. In FIG. D.1(d) the *slopes* of the measured data (black markers and 1(a)) and calculated values (red markers) agree well. This agreement indicates that the span of matrix ion intensities observed in data from the standard analyses was primarily driven by variable charging in the DLC matrix. In contrast, in FIG. D.1(d) the order of the measured intensity data is different from the calculated intensities. There are several possible reasons for this discrepancy. For example, the 2009 energy spectra might not have been centered exactly on a "STD_3-type" matrix as assumed, or the measured intensities might reflect unrecorded variations in beam current during the analyses. However, we believe that the primary variation in the order of the standards is that *the calculation does not consider differences in ion yields for the various matrix types* (see FIG. 2 in text). For example, STD_7 has a significantly higher ion yield than most of the other analyses (FIG. 2 in main text) because of the silicon present.

So, the slope of the matrix ion intensities and the differences between the observed and calculated order of analyses along that slope can be explained by the matrix effects in the DLC. The only remaining difference between the measured data and the calculated values in FIG. D.1(d) is that the measured data seem to have a slightly (but systematically) higher $^{12}C_2^+$ intensity. It is not clear if the difference is within the errors of measurement/calculation. But, if the increased intensity of the measured $^{12}C_2^+$ intensity is real, then that difference could be an artefact. For example, perhaps the sample preparation before SIMS analysis etched sp^2 bonds from the surface of the DLC during cleaning. Or, perhaps, settings in the SIMS may have resulted in a slightly higher $^{12}C_2^+$ intensity due to scattering of $^{24}Mg^+$ ions at the from surface contamination (energy spectra were taken at the pre-sputtered surface). Unfortunately, artefacts are impossible to resolve at this point because these spectra were taken more than a decade after the actual analyses.

E. Effect of Changing the Compound Correction of the SRIM Model: e.g., STD_4

In general, it is the atoms that give the stopping power of the matrix. However, when bonds are strong, they may contribute to the stopping power. This is especially true in carbon matrices because there are three bond types (single, sp^2, sp^3) which have dramatically different electrical properties. Specifically, a glassy carbon is very different from graphite, and even more dissimilar when compared to diamond. SRIM is not designed to deal with bond differences at a fundamental level. Instead, it uses the "core and bond" method" (Ref. [3]), where the stopping power is calculated using the atomic core and empirical "compound correction", which is usually 1 (a description of the weakest possible bond of the matrix; e.g., C-C bonding in carbon). This "compound correction" decreases linear with an increasing contribution of stopping power from bonds. But, the change in the compound correction with the amount of increased stopping power from bonds must be found empirically, through experiment. The reason for this is that the effect of the bonding on stopping power is affected by the ability of the matrix to

dissipate the electrical energy from the incoming ions, and this effect will change with the texture (distribution of bonds) of the material as well as the concentration of the bonds.

Changing the compound correction in SRIM does change the quality of the best fits to our data. For example, it was determined that the "906 Nuclear Grade *Graphite*" fit the standard better than a plain carbon matrix; yet, a carbon matrix was a better fit for the SW depth profiles. Of course, the SW collectors contain a small percentage of hydrogen, and the hydrogen atoms will tend to lower the overall stopping power (both because H has intrinsically less stopping power than C and because C-H bonding is weaker than sp^2). In fact, the compound correction does not seem to have a dramatic effect on the shape of the SRIM model, but it does have a significant effect on the calculated density. This is shown in FIG. E.1 for two models of the ^{24}Mg in STD_4, where the yellow SRIM model has a compound correction of 0.8684 (#906 Nuclear Grade Graphite) and gives a density of 2.85 gm/cm^3 and the red SRIM model has a compound correction of 0.7986 (sp^3 vs. sp^2 bonds – see Core and Bond Theory on [3]) and gives a density of 3.0 gm/cm^3.

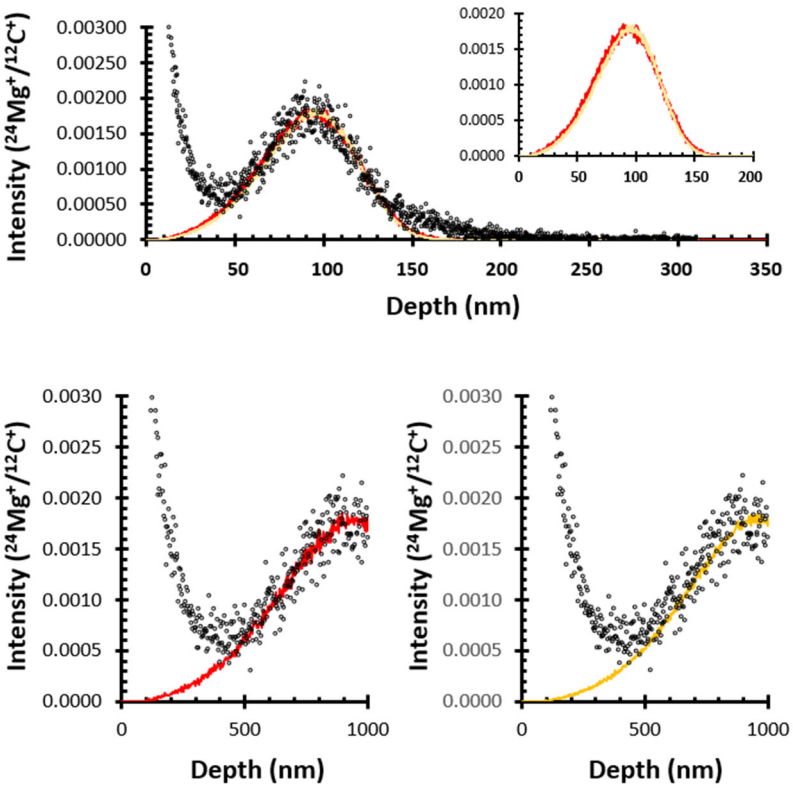

FIG. E.1*. $^{24}Mg^+$ depth profile (black) of STD_4 and two SRIM models that fit the data. One uses a compound correction 0.8684 and a density of 2.85 gm/cm^3 (yellow) and the other uses a compound correction of 0.7986 and a density of 3.0 gm/cm^3 (red).*

F. Effect of a Lower Ion Beam Density on a Diamond-like matrix: e.g., STD_4 after Ref. [4]

Most SIMS analyses are done in silicon or in geological materials that are silicon-based. Therefore, when we choose conditions for analyses, silicon is the substance on which our intuition is based. Working with diamond-like carbon is non-intuitive for most of us. The first author believes that an example of that quirkiness is the difference in the range of energies and ion densities that define the range of dynamic SIMS in DLC vs. silicon. Some of the discussion of the ion density that defines dynamic SIMS is given in the text (Section IV C. Relevance of Results to DLC structure). Another line of evidence is the experiment described below at the start of the STD_4 analysis.

The point beam used for these analyses had a "wing" on it. That "wing" produced lots of secondary ion scatter, and so the DTOS image was circumscribed with the field aperture, which successfully eliminated secondary ions from outside the analysis area. However, at the initiation of the STD_4 analysis, the first author tried using a small, but finite, spot for the focus instead of the point beam. The raster sweep was kept the same, but the bigger beam spot should have made the raster itself slightly larger. DTOS was not refocused so fewer counts were expected, but the field aperture would have kept the image field the same. Other conditions were also kept the same.

The result is in FIG. F.1. Effectively, the data was extremely different when a small spot beam was used instead of a point beam. The dashed vertical line in FIG. F.1 marks the time of refocus back to a point beam (LHS of vertical line = finite spot beam; RHS of vertical line = point beam). Initially, while the beam was focused as a spot:

(1) both the $^{12}C_2^+$ and $^{12}C^+$ intensities were lower, as expected, but the $^{12}C_2^+$ intensity was nearly double that of the $^{12}C^+$ intensity,

(2) $^{24}Mg^+$ intensity was lower than after the refocus,

(3) $^{25}Mg^+$ intensity (= ($^{25}Mg^+$+$^{24}Mg^+H$) intensity) was significantly higher than the $^{26}Mg^+$ intensity before the refocus, but about the same as the $^{26}Mg^+$ intensity (which is what it was supposed to be) after the refocus.

(4) $^{26}Mg^+$ intensity remained effectively unchanged.

In summary, $^{24}Mg^+$ and $^{12}C^+$, the two masses without singly- or doubly-charged molecular interferences, both dropped in intensity, molecular carbon intensity decreased, but proportionately less than $^{12}C^+$, the intensity at mass at 25 increased, suggesting more ^{24}MgH and possible some doubly-charged molecular interferences, too. The addition of molecular interferences at mass 26 could, conceivably, also explain why the mass 26 did not decrease. One possible explanation for this weird result is that the lower ion beam density didn't fully break all of the bonds of the matrix, and this spot beam was near the threshold of ion density

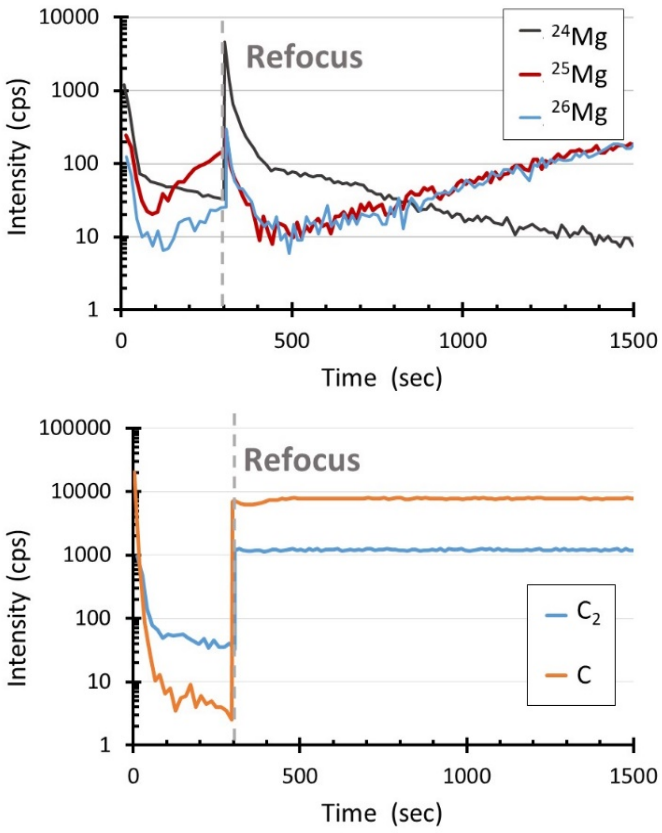

***FIG. F.1**. Depth profiles from the matrix of STD_4 using a small spot vs. a point beam. Vertical line is when the small spot was focused to a point. Ion species as marked in the legend.*

for dynamic SIMS because of the unique bonding state of the matrix of STD_4. That analysis, as mentioned previously and discussed in the text (Section IV B. Relevance of the C_2^+/C^+ parametrization), had the highest $^{12}C_2^+$ / $^{12}C^+$ ratio (0.153) and it was on the verge of charging ***after*** the refocus. It is not clear what the spot (slightly defocused) beam did to the voltage of the matrix. Ideally, a less dense ion beam over a slightly larger area should have decreased the voltage; but DLC, is not an ideal conductor, so the answer is not clear. However, ion density was definitely lower, albeit no more than a factor of two since the raster was already 250 µm^2.

To check this possibility, we assume that C reflects the sputtering rate of the matrix and perform a rough calculation. For simplicity, assume operator error made that "small" spot 50 µm in diameter. Then the size of the raster would have been (250+50 µm^2). Since the area of the raster would have increased by 44%, the new ion density would have been ~1.5E14. Moreover, if sputtering rate is a linear function of the rastered area, the sputter rate would have gone from 0.0215 nm/sec to 0.015 nm/sec and, ideally, the C counts would have dropped proportionally from ~10000 cps to ~1500 cps. But, the defocused ion beam was only giving ~3cps C. Even if 90% of the secondary ions had been screened because the field aperture masked most of the focused DTOS point, 10% (or ~150 cps) should have been transmitted, but we only see ~3 cps. If 3 cps of $^{12}C^+$ reflects sputtering rate, then (0.015/150) x 3 = 1 nm/hr. That is, sputtering with the "defocused" beam is transitional between static sims and dynamic sims sputtering regimes. That result would explain both the low C counts and the relative increase in counts at masses that may include molecular ions. In addition, note that if the counts were low only due to charging (see FIG. D.1(d) and Table D.1 footnote e) then the $^{12}C_2^+$ should go to zero before $^{12}C^+$.

G. Notes and References

§. In a uniformly conductive material, the "0 offset" of the energy spectra are set once, simply to insure maximum counts for each subsequent analysis. However, when the electrical conductivity of the sample changes in a non-uniform material (e.g., DLC), these voltage offsets are realized as a function of the electrical conductivity, as detailed in Section 4.1 of the text.

§§. As DLC approaches the (low) electrical conductivity of diamond, during SIMS analysis it begins to act more like a silica-based glass than a graphite-rich composite. When the voltage increases significantly, the low electrical conductivity allows charge buildup in the sample which, when it becomes excessive, causes loss of the secondary-ion signal. The only profile that has a $^{12}C_2^+$ / $^{12}C^+$ value within the red gradient is STD_4. In the main text and in Section E of this Appendix, we give reasons supporting the speculation that the matrix of STD_4 was primarily nanodiamond.

1. Sullivan J. P., Friedmann T. A., Dunn R. G., Stechel E. B., Schultz P. A., Siegal M. P. and Missert N., "The electronic transport mechanism in amorphous tetrahedrally-coordinated carbon films," Materials Research Society Symposium Proceedings 498: 97-102 (1998).

2. Chu P. K. and Li L., "Characterization of amorphous and nanocrystalline carbon films," Materials Chemistry and Physics, 96: 253–277 (2006).

3. www.srim.org (Core and Bond Theory is under "Tutorials").

4. Jurewicz A. J. G., Burnett D., Rieck K., Hervig R., Friedmann, T., Williams P., Daghlian C. and Wiens R., "Understanding heterogeneity in Genesis diamond-like carbon film using SIMS analysis of implants," Journal of Materials Science 52(19): supporting online materials, Open Access (2017).